StAR-like Activity and Molten Globule Behavior of StARD6, A Male Germ-Line Protein†

Himangshu S. Bose,*,‡ Randy M. Whittal,§ Yong Ran,‡ Mahuya Bose,‡ Bo Y. Baker,|| and Walter L. Miller⊥

Department of Physiology, University of Florida, Gainesville, Florida 32610, Department of Chemistry, University of Alberta, Edmonton, Alberta, T6G 2G2 Canada, Infectious Disease Division, Menzies School of Health Research, Darwin, Northern Territory, Australia, and Department of Pediatrics, University of California, San Francisco, California

Received October 1, 2007; Revised Manuscript Received December 12, 2007

ABSTRACT: The steroidogenic acute regulatory protein (StAR) belongs to a family of 15 StAR-related lipid transfer (START) domain proteins termed StARD1−StARD15. StAR (StARD1) induces adrenal and gonadal steroidogenesis by moving cholesterol from the outer mitochondrial membrane to the inner mitochondrial membrane by an unclear process that involves conformational changes that have been characterized as a molten globule transition. We expressed, purified, and assessed the activity and cholesterol-binding behavior of StARD1 and StARD3−D7, showing that StARD6 had activity equal to StARD1, whereas StARD4, D5, and D7 had little or no activity with adrenal mitochondria in vitro. Partial proteolysis examined by mass spectrometry suggests that StARD6 has a protease-sensitive C-terminus, similar to but smaller than that of StARD1. Experiments using urea denaturation, stopped-flow kinetics and measurements of mitochondrial membrane association suggests that StARD1 and StARD6 both unfold and refold slowly with similar kinetic patterns. Isothermal titration calorimetry suggests that StARD6 interacts with mitochondrial membranes as well as or better than StARD1. Computational modeling of StARD6 suggests that it has a similar fold to StARD1, with a hydrophobic sterol-binding pocket and a unique C-terminal extension. StARD6, which is expressed only in male germ-line cells, thus exhibits biological and biophysical properties that imply a role in steroidogenesis.

The steroidogenic acute regulatory protein (StAR) is a 37 kDa phosphoprotein that facilitates the movement of cholesterol from the outer mitochondrial membrane (OMM[1]) to the inner mitochondrial membrane (IMM), where cytochrome P450scc converts cholesterol to pregnenolone (*1*). StAR is an essential protein in mammals and possibly in other vertebrates, mediating the acute steroidogenic response. Absence of StAR causes potentially lethal congenital lipoid adrenal hyperplasia (lipoid CAH) in infancy (*2*, *3*), and StAR-knockout mice faithfully reproduce the human phenotype (*4*, *5*). StAR is the first-described member of a family of proteins that contain so-called START (StAR-related lipid transfer) domains, which can be found in a broad array of species from birch trees to humans (*6*). Fifteen START domain proteins appear to serve roles in binding and transferring lipids in mammals, and are called StARD (START domain) proteins (*7*). The crystallographic structures of the START domains of StARD3 (N-216 MLN64) (*8*) and StARD4 (*9*) are very similar, and computational models show that StARD1 has a virtually identical three-dimensional structure (*10*−*12*). These structures all feature a prominent C-helix, which appears to be the only domain that interacts with OMM lipids (*11*). Although StAR (StARD1) is the only member of this family proven to transfer cholesterol into mitochondria in vivo (StAR activity), the START domain of StARD3 has about 50% of StAR activity in vitro (*13*, *14*) and StARD4 has trace activity while StARD5 has none (*15*). Based on its linear sequence, StARD6 falls into a small subfamily of StARD proteins comprising StARD4, StARD5 and StARD6 (*7*, *16*) and appears to be exclusively expressed in the male germ cell line (*7*, *17*, *18*), but has not been studied functionally. We sought to compare structures, StAR-like activity, and cholesterol-binding capacity of these proteins. Our data show that StARD6 behaves very similarly to StARD1.

EXPERIMENTAL PROCEDURES

Subcloning of START Proteins. The cDNAs for human StARD1 and StARD3 and mouse StARD4, StARD5, StARD6, and StARD7 were subcloned into pQE30 by PCR amplification of the cloned template as described (*14*) using Taq polymerase (Promega, WI) and the primers listed in Table 1. The PCR-amplified cDNA was purified by agarose gel electrophoresis, digested with *Bam*HI/*Eco*RI or *Bam*HI/*Kpn*I, ligated to predigested pQE30 vector, and transformed into

† This work was supported by grants from Pfizer, March of Dimes, the American Heart Association and the start up package to H.S.B. and NIH Grant DK37922 to W.L.M.

* To whom correspondence should be addressed. Department of Physiology and Functional Genomics, College of Medicine, University of Florida, 1600 SW Archer Road, Room M552; Box 100274, Gainesville, FL-32610. Tel: 352 392 3243. Fax: 352-846-0270. E-mail: hbose@ufl.edu and himangshubose@hotmail.com.

‡ University of Florida.

§ University of Alberta.

|| Menzies School of Health Research.

⊥ University of California, San Francisco.

[1] Abbreviations: CD, circular dichroism; UPLC, ultra performance liquid chromatography; IMM, inner mitochondrial membrane; LCMS, liquid chromatography/mass spectrometry; OMM, outer mitochondrial membrane; StAR, steroidogenic acute regulatory protein; START, StAR-related lipid transfer.

10.1021/bi701966a CCC: $40.75 © 2008 American Chemical Society
Published on Web 01/23/2008

Table 1: Oligonucleotides Used for Subcloning in *E. coli* Expression Vector

StARD1	
sense	5′AGCTA**GGATCC**ATGCTGCTAGCGACATTCAAG3′
antisense	5′AAGCT**AGAATTC**T CAACACCTGGCTTCAGAGGC-AGG3′
StARD4	
sense	5′ATA**GGATCC**ATGGAAGGCCTGTCTGATGT3′
antisense	5′GCG**GGTACC**TCATAA AGCTTTTCGTAAAT3′
StARD5	
sense	5′ATAA**GGATCC**ATGGACCCTGCACTGGCA3′
antisense	5′GCG**GGTACC**TTACTCA TGGAATTGCTT3′
StARD6	
sense	5′AGA**GGATCC**ATGGACTATAAGGCTATCGC3′
antisense	5′AGA**GGTACC**CTACGG TTTAATGGCAGAAT3′
StARD7	
sense	5′ATT**GCATGC**ATGGCGGCGTTAGCCGGCGTCTT
antisense	5′CGC**AAGCTT**TC AAGCATACTCAATCCGAGCA

Escherichia coli M15. The sequence of each construct was verified on both strands.

Protein Expression and Purification. Transformed *E. coli* were grown with ampicillin and kanamycin at 37° to an optical density of 0.5, then transferred to 15 °C, induced with 0.4−1 mM IPTG, and allowed to grow for an additional 12 h. Bacterial pellets containing the expressed START domains were resuspended in lysis buffer (50 mM NaH_2PO_4, 300 mM NaCl, and 10 mM imidazole, pH 8.0) and sonicated with 10 s pulses and 30 s rests for 10 min. The soluble fraction was separated by centrifuging at 15000*g* for 30 min, then passed through a Ni-NTA column washed first with lysis buffer then with 50 mM NaH_2PO_4, 300 mM NaCl and 25 mM imidazole, pH 8.0. The column was then eluted with 250 mM imidazole, pH 7.5. The eluates were dialyzed against 20 mM NaH_2PO_4, 50 mM NaCl pH 7.4, then the proteins were purified through a gel-filtration column connected to a FPLC, and the concentrations of the unfolded proteins were determined with guanidinum hydrochloride to avoid errors in extinction coefficients (*19*). For the determination of bioactivity, the purified proteins were supplemented with 10% glycerol. The proteins remained fully active for approximately four weeks.

Circular Dichroism. Far-UV (195−250 nm) circular dichroism (CD) measurements were carried out in an Aviv-215 spectropolarimeter at 20 °C with a 1.0 mm path length, rectangular cuvette containing 175 μg/mL (1.52×10^{-6} M) protein in 10 mM Tris-HCl, pH 7.5. Spectra shown are averages of three consecutive scans that were performed at a scan speed of 10 nm/min and corrected by subtracting corresponding buffer blanks. Results are presented as mean residue molar ellipticity (Θ): $[\Theta]_r = \theta_{obs}/(10nlc)$, where θ_{obs} is the measured ellipticity in millidegrees, n the number of residues in the protein, l the path length of the cell expressed in cm, and c the molar concentration of protein. Data were collected every 1 nm with a 1 nm bandwidth, and the helical content was estimated using the program CD pro (*20*−*23*).

StAR-like Activity Assays. Biosynthetic START domains were added to pig adrenal mitochondria (10 μg of mitochondrial protein) in a final volume of 100 μL of bioassay buffer (125 mM sucrose, 80 mM KCl, 5 mM $MgCl_2$, 10 mM NaH_2PO_4, 10 mM isocitrate, 25 mM HEPES, 0.1 mM ATP, and 10 μg/mL cholesterol, pH 7.4) (*24*). The mixture was then incubated for 1 h at 37 °C, and pregnenolone synthesis was measured by radioimmunoassay.

Cholesterol Binding. Purified START proteins (1 μM) in phosphate buffer were incubated with various concentrations of NBD-cholesterol (Molecular Probes/Invitrogen) for 15 min at 37 °C, and fluorescence emission maxima were measured on a Shimadzu fluorescence spectrophotometer (Shimadzu, model 5301 PC) as described (*25*, *26*). The NBD-cholesterol was excited at 460 nm, and the emission maxima were recorded at 534 nm. The collected data points were processed using Kaleidagraph or Microcal Origin (Origin Lab, MA).

Proteolytic Digestion and Mass Spectrometry. Limited proteolytic digestion experiments were performed at room temperature or 4 °C using 5 μg of START proteins and different concentrations of trypsin (sequencing grade, Promega) for various periods of time. The reactions were terminated with an equal volume of SDS-sample buffer containing 2 mM PMSF and transferred to a boiling water bath. Following electrophoresis, the samples were stained with Coomassie brilliant blue or silver nitrate, individual bands were excised, destained, reduced with DTT (Roche), alkylated with iodoacetamide (Sigma) and digested with trypsin (Promega Sequencing Grade Modified) overnight (*27*). The extracted peptides were analyzed by mass spectrometry via LC MS/MS on a nanoAcquity UPLC (Waters, MA) coupled with a Q-ToF-Premier mass spectrometer (Micromass, U.K./Waters, MA). Tryptic peptides were separated using a linear water/acetonitrile gradient (0.1% formic acid) on a nano Acquity column (3 μm Atlantis dC18, 100 Å pore size, 75 μm i.d. × 10 cm) (Waters, MA), with an in-line Symmetry column (5 μM C18, 180 μm i.d. × 20 mm) (Waters, MA) as a loading/desalting column. Protein identification using the generated MS/MS spectra was performed by searching the NCBI nonredundant database using Mascot MS/MS Ion Search at www.matrixscience.com (Matrix Science, U.K.) with consideration for the carbamidomethylation of cysteine and the oxidation of methionine.

Urea-Induced Denaturation. Equilibrium unfolding of START domains was monitored by fluorescence and CD measurements as a function of urea concentration. Protein samples (0.3 mg/mL for CD; 0.04 mg/mL for fluorescence) were equilibriated with different concentrations of urea overnight at room temperature. Data were collected every 1 nm with a 1 nm bandwidth, and the helical content was estimated using the program CD pro (*20*−*23*). Fluorescence was measured using a Shimadzu RF-5301PC spectrofluorophotometer; samples were excited at 280 and 295 nm, and data were collected at 295 to 450 nm in 0.2 nm intervals. The urea-induced unfolding of START domains was monitored by fluorescence spectroscopy excited independently at 280 and 295 nm with emission measurement at 320 nm. CD and fluorescence spectroscopy data were processed with Origin 5.0 (Origin Lab, MA).

Stern−Volmer Fluorescence Quenching. To examine the surface exposure of Trp in StARD1, D3, D4, D6 and D7, fluorescence quenching experiments were performed by successively adding 2 μL aliquots of 2 M acrylamide to 1 μM protein solution and by monitoring the change in Trp emission intensity at 340 nm. To correct for acrylamide absorption (295 nm), the measured intensity was multiplied by the antilog of OD/2, where OD is the optical density at 295 nm and 0.5 cm is the effective path length of the cell. The Stern−Volmer quenching constant (K_{SV}) was calculated as the slope of the linear region of the F_0/F_{corr} vs [Q] plots,

where F_0 and F_{corr} are the corrected fluorescence intensities in the absence and presence of different concentrations of quencher molecule, respectively (*25*, *28*, *29*).

Stopped-Flow Spectrophotometry. The kinetics of protein unfolding were measured in an AVIV spectropolarimeter interfaced with an SF3 stopped-flow module (Biologic, France). A stock concentration of each START protein (3 mg/mL) in the syringe was changed to 0.6 mg/mL in the cell. The protein solution (36 μL) and 10 M urea (144 μL) were mixed with a "Delta" mixer. The syringes were operated at 3 mL/s with a 9.7 ms dead time. Fluorescence was measured by excitation at 280 nm with emission intensity using a 320 nm cutoff filter. Data were collected in four segments. First, 40 data points were collected to monitor the basal signal of the solution. Second, the solution was mixed for 60 ms. Third, 100 data points were collected over 100 ms to monitor initial rapid kinetics, then 200 data points were acquired over a 2 s time period to monitor slow kinetics. Data were fitted to a two-exponential decay equation: $I = I_0 - \sum e^{-kt}$, where I is the intensity at any time, I_0 is the initial intensity, k is the unfolding rate constant and t is the time (*30*).

Isothermal Titration Calorimetry. Mitochondria were prepared as described (*31*), and 0.3 mg of mitochondrial protein was suspended in 1.5 mL of buffer containing 125 mM sucrose, 80 mM KCl, 5 mM $MgCl_2$, 10 mM NaH_2PO_4 10 mM isocitrate, 1.0 mM ATP, 1.0 mM NADP, 0.1 mM ADP, 25 mM HEPES pH 7.4, and 10 μg/mL cholesterol. This buffer was prepared without cholesterol, and a stock solution of 40 mg/mL cholesterol in methyl-β-cyclodextrin was added by serial dilution. The mixture was titrated with increasing amounts of StAR protein from a stock solution of 100−700 μg/mL in a MicroCal VP-ITC calorimeter (Northhampton, MA) equipped with an automatic injector. Control experiments were done with isolated mitochondria plus cyclodextrin without cholesterol, mitochondria plus cholesterol and a mixture of mitochondria, cholesterol and heat-denatured StARD1. All buffers were filtered and degassed before use. Data were collected by incubating the mitochondria in the cell for 2 h prior to the injection of 5 μL aliquots of protein at speed of 0.5 μL/s with an equilibration time of 7 min between injections. Enthalpy changes (ΔH) were measured by integration of excess power generated by the reaction divided by the concentration of the injectant:

$$\Delta H = \int P \, dt/[S]_t v^\circ$$

where P is the excess power, v is the volume (of the calorimeter cell), and [S] is the concentration of the injectant.

Homology Modeling of Mouse StARD6. The sequence of mouse StARD6 (GenBank Accession No. AF480303) was aligned with the sequences of mouse StARD4 and StARD3 (N-216 MLN64) using the program CLUSTALW. STARD6 has higher identity (27%) and similarity (56%) to StARD4 than to StARD3 (23% in identity and 41% in similarity). Therefore, we used the mouse StARD4 structure (PDB ID: 1JSS) as a template to model the main structure of StARD6. Compared with other StAR proteins, StARD6 contains a C-terminal extension comprising residues of 210 to 233, which do not align with structures in START domains. To infer structural information for this region, we did a BLAST search of residues 210 to 233 (the "C-tail") of StARD6 against the Protein Database. The best match was a segment of anti-morphine antibody 9b1. The C-tail of StARD6 has 56% sequence identity and 64% similarity to residues 186 to 207 of the light chain of 9b1 (PDB ID: 1Q0X). An alignment of C-tail StARD6 to 1Q0X is shown below:

```
StARD6  RA - - RHSSHSS -V -HKKKEGHSAIK
1Q0X:   RAWERHSSYSCQVTH- - -EGHSSNK
```

Therefore, segment 186−207 of 9b1 was used as a template to construct the conformation of residues 210 to 233 of StARD6. The resulting alignment was examined manually and was submitted for automated modeling using MODELLER 8v1 (*32*). Twenty models were initially generated and evaluated with DOPE energy calculation in MODELLER. The C-terminal region of StARD6 contains a proline at 189 which should break the long C-helix. The models with lowest value of the MODELLER objective function were chosen for further model refinement on the C-terminal region. A hundred models were generated, and one of the lowest values of DOPE at the C-helix was selected as the final model for further energy minimizations.

The potential energy of the initial StAR model was minimized using the AMBER7 (*33*) program with amber force field ff94 (*34*) plus the modified frcmod.mod_phipsi.2 file at the Computer Graphics Laboratory at University of California at San Francisco. Briefly, the model of StARD6 has a net charge of +12 and was neutralized and solvated using the pre-equilibrated TIP3P water model in a rectangular box with a minimum solute−wall distance of 10 Å. Energy minimization was performed with a steepest descent energy minimization (1000 steps) with positional restraints on the protein and second minimization (1000 steps) on the whole system. The free energy of the structure reached the local minima after the run. The resulting model was checked using the program Procheck and WhatIf (www.cmbi.kun.nl.gv.servers/WIWWWI/). The figures were generated with Chimera (*35*). A short molecular dynamics (MD) simulation was done to explore the conformation of the C-tail region of muStARD6. After energy minimization, the whole system was heated to 300 K over 100 ps. Then the MD was run under constant temperature and pressure for 100 ps with the restraints switched off. The system energy, temperature, and pressure were checked before and after each MD run.

RESULTS

Expression of START Domain Proteins. To study the activity and structure of START proteins, we first expressed and purified milligram quantities of the START domains of StARD1, D3, D4, D5, D6 and D7 (Figure 1A). Each soluble protein was purified from bacterial cytosol first by nickel affinity chromatography using our previously described protocol (*14*, *36*), and second through FPLC. Western blotting using an antibody directed to the His-tag showed that the proteins were of the expected size (Figure 1B). As a general indicator of the similarities or differences in the three-dimensional structures of these bacterially expressed proteins, we performed far-UV CD spectroscopy (Figure 1C). Subtractions of the buffer spectra from the experimental samples showed no absorption of all the proteins at 250 nm. The spectra of StARD3, D4, D5, and D6 were very similar

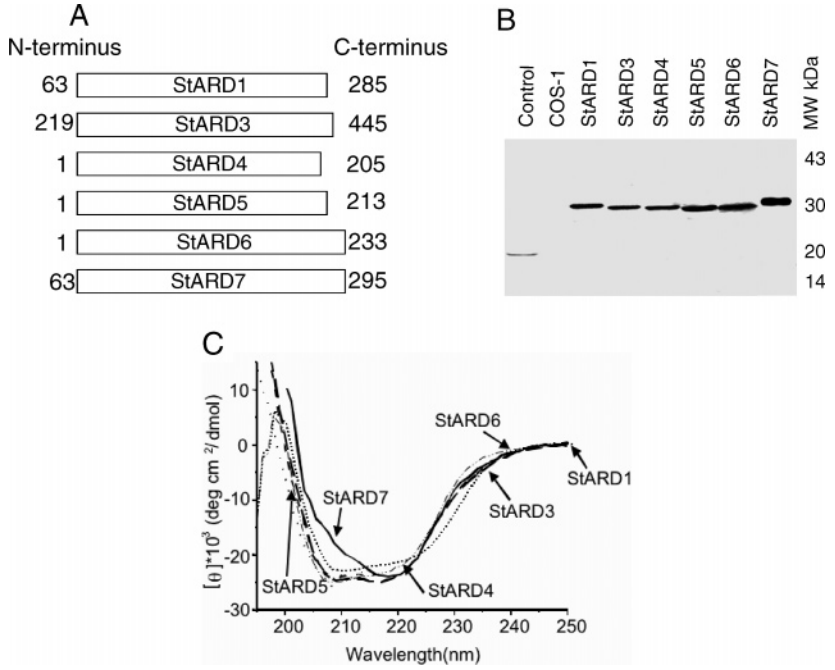

FIGURE 1: Preparation and characterization of START domain proteins. Panel A. Schematic diagram of the different START domain proteins used showing the amino acid numbers of the N- and C-termini. Panel B. Western blot of purified proteins run on a 15% acrylamide gel and probed with an anti-His-tag antibody. Panel C. Equilibrium CD spectra of StARD1 (— — —) StARD3 (—•—), StARD4 (— - - —), StARD5(- - -), StARD6 (•••) and StARD7 (—) recorded from 195 to 250 nm.

Table 2: Secondary Structural Analysis of the START Domain-Containing Proteins

	α-helix (%)		β-sheet (%)	
protein	crystal	CD	crystal	CD
StARD1		26		23
StARD3	26.7	24.7	37.4	31.0
StARD4	24.6	21.0	42.2	29.5

Calculation from CD Spectra

protein	helix (%)	sheet (%)	turn (%)	coil (%)
StARD4	21.0	29.5	22.1	27.2
StARD5	21.4	32.9	19.7	26.1
StARD6	24.0	29.8	20.8	26.4
StARD7	3.7	34.4	28.1	33.3

to the spectrum of StARD1, which was indistinguishable from our previously published spectra of this protein (*36*, *37*). These proteins had minima at 208 and 222 nm, typical of an α-helical conformation; by contrast, StARD7 had a minimum at 218 nm, typical of a predominantly β-sheet conformation (*38*). These calculations encompassed the CD data from 185 to 240 nm, except in the case of StARD7, where there was a high signal-to-noise ratio below 195 nm, so that below 195 nm we extrapolated to match the data with the other StARD proteins. Calculations of secondary structural characteristics by the program CD pro (*20*, *23*) indicated that, with the exception of StARD7, the proteins were predicted to have similar helical contents to the known crystal structures of StARD3 and StARD4 (Table 2).

StAR-like Activities of the START Domain Proteins. The biological role of StARD1 in the mitochondrial import of cholesterol for steroidogenesis is well-established (*2*, *3*); StARD3 (MLN64) appears to play a similar role in endosomes (*39*), but the biological roles of StARD4, D5, D6 and D7 remain speculative (*7*). To determine whether any of these proteins possesses StAR-like activity, we incubated 1 μg of each protein with isolated pig adrenal mitochondria and measured pregnenolone synthesis (Figure 2A). As previously described, the START domains of StARD1 (N-62 StAR) and StARD3 (N-216 MLN64) had similar activities and those activities were less than the maximal steroidogenic capacity of the mitochondria, which was determined by adding 5 μM 22R-hydroxycholesterol (*14*). Addition of the biologically inactive StARD1 mutant R182L (*3*, *40*) or of StARD5 or StARD7 elicited no more activity than buffer alone; StARD4 had a low level of StAR-like activity, as expected (*15*), but StARD6 had activity equal to that of StARD1 or StARD3. Thus the biological roles of StARD4, StARD5 and StARD7 are most likely unrelated to the mitochondrial import of cholesterol, but the robust activity of StARD6 in this assay suggests that this protein may serve a similar role to StARD1.

To characterize the activities of these proteins in more detail, we examined activity as a function of the concentration of added protein and as a function of incubation time. Using a constant amount of mitochondrial protein and a 1 h incubation time, increasing the amount of added StARD1 elicited a maximal steroidogenic response (about 220 ng of pregnenolone/mL) with only 2.5 μg of protein (Figure 2B). StARD5 and StARD7 elicited no response, and StARD4 elicited a minimal response, consistent with Figure 2A. Although StARD3 exerted a nearly maximal response at 2.5 μg, a further increase (to about 280 ng of pregnenolone/mL) was seen with 10 μg of protein. By contrast, StARD6 exerted similar activity to StARD1 and StARD3 at 2.5 μg, but the effect increased in a dose-dependent fashion to a nearly maximal value of about 700 ng of pregnenolone/mL at 10 μg of protein. Thus StARD6, which is expressed only in the male germ cell lineage (*17*), appears to be a more potent StAR-like factor than StARD1, suggesting that StARD6 may act on mitochondrial cholesterol import. Therefore we focused attention on StARD6.

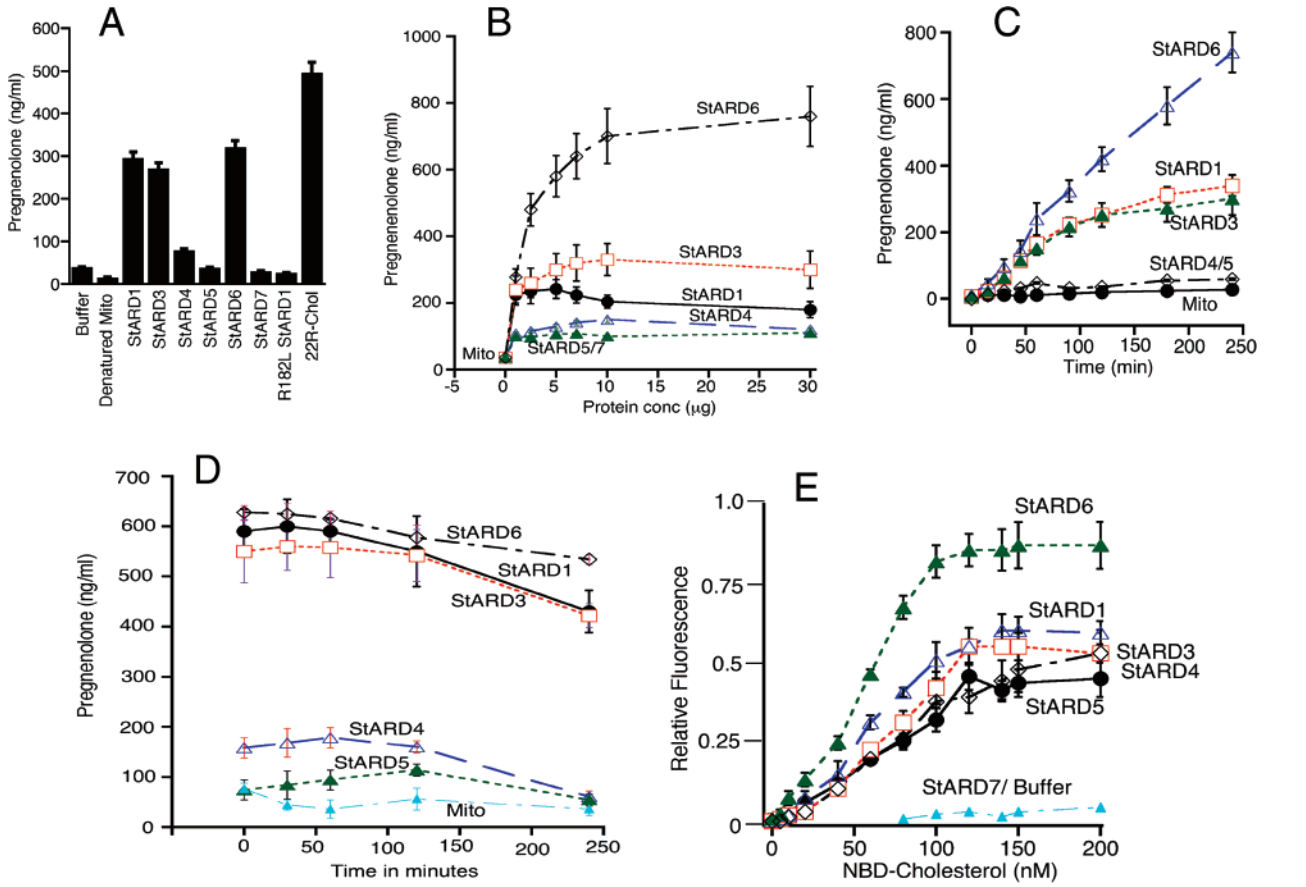

FIGURE 2: StARD6 exhibits robust StAR-like activity. Panel A. Accumulated pregnenolone synthesis from pig adrenal mitochondria incubated with the biosynthetic StARD1, StARD3, StARD4, StARD5, StARD6, and StARD7 for 1 h. Panel B. Effect of protein concentration on pregnenolone synthesis. Increasing concentrations of the START domain-containing proteins were incubated with a constant amount of mitochondria (10 μg of mitochondrial protein) for 1 h. Panel C. Kinetics of pregnenolone accumulation. Equal amounts of biosynthetic proteins were incubated with mitochondria (10 μg of mitochondrial protein) for up to 4 h. Panel D. Stability of different StAR proteins. Constant amounts of START proteins were preincubated at 37 °C for the times indicated, then added to mitochondria and pregnenolone synthesis was measured after 60 min. Panel E. Binding of START proteins to increasing concentrations of NBD-cholesterol. The relative intensity of the fluorescence intensity maximum at 560 nm was plotted against NBD-cholesterol concentration. In all panels, data are mean ± SEM from 3 or 4 independent experiments, each performed in triplicate.

As a control experiment, we examined the "viability" of the isolated mitochondria by measuring pregnenolone synthesis for up to 4 h (Figure 2C). Consistent with Figures 2A and 2B, StARD4 and StARD5 had essentially no more effect after 4 h than they did after 1 h. By contrast, StARD1, StARD3 and StARD6 elicited further steroidogenesis, as evidenced by accumulating pregnenolone in the assay medium. Most interestingly, the effect of StARD6 was linear with time for up to 4 h, whereas the effects of StARD1 and StARD3 diminished with time. These data show that the isolated mitochondria remained viable for at least 4 h and are not limiting in the assays, and suggest that StARD1 and StARD3 were slowly inactivated, whereas StARD6 was not. To assess the stability of the START domain proteins, we preincubated them for 0−4 h in buffer at 37 °C before adding them to mitochondria for 1 h and measuring pregnenolone production (Figure 2D). Consistent with Figure 2C, StARD6 activity diminished only ~10% with preincubation, whereas StARD1 and StARD3 lost about 25−30% of activity.

Although cholesterol binding does not predict StAR-like activity (*40*), we sought to determine whether these START domain proteins could bind cholesterol. StARD1 binding of authentic [^{14}C]cholesterol and the somewhat larger fluorescent compound NBD-cholesterol is equivalent (*40*), hence we used assays with NBD-cholesterol. The START domain proteins we studied are of very similar sizes, and we used the same amount of protein throughout the experiment, thus the relative change in fluorescence should be proportional with the binding of NBD-cholesterol. The binding assays yielded sigmoidal curves, as expected (*25*), showing that StARD1 and StARD3 bound cholesterol equivalently, and StARD6 bound about 1.5 times as much NBD-cholesterol as StARD1 or StARD3 (Figure 2E). As StARD1 and StARD3 bind cholesterol with nearly 1:1 stoichiometry (*8*), it would appear that StARD6 may be able to bind more than one molecule of cholesterol. Others have reported that StARD1 bound NBD-cholesterol with 2:1 stoichiometry (*25*); while we have not observed this, it is possible that the NBD group of NBD-cholesterol binds to the surface of StARD6 as well as to its sterol-binding pocket.

To investigate the higher binding efficiency of StARD6 with NBD-cholesterol, we examined the Trp environment of these StARD proteins by acrylamide quenching of Trp residues, as a means of surveying the surface characteristics of the proteins. Acrylamide is an electron-deficient compound that deactivates the radiative pathways of excited fluorophores by collisional quenching (i.e., electrons are transferred from the excited indole group to acrylamide). This quenching

effect allows one to detect minor structural differences in protein molecules, since proteins with greater Trp accessibility and higher acrylamide binding undergo a greater decrease in fluorescence intensity. The Stern−Volmer constant, K_{SV}, which provides an index of quencher accessibility, was calculated for all the proteins based on the fluorescence intensity for each. For reference we employed the model Trp compound *N*-acetyl-L-tryptophanamide (NATA), which has an open chain conformation with a K_{SV} value of 16.5 ± 0.3 M^{-1}. At an excitation of 295 nm, the K_{SV} of StARD1 was 11.3 ± 0.2 M^{-1}, StARD3 was 10.3 ± 0.5 M^{-1}, StARD4 was 10.5 ± 0.2 M^{-1}, StARD6 was 10.9 ± 0.3 M^{-1} and StARD7 was 10.3 ± 0.2 M^{-1}. Since StARD5 has five Trp residues, whereas StARD1, D3, D4, D6, and D7 have four, we could not compare the K_{SV} of StARD5 in the present experiment. These results suggest that surface exposures of the Trp residues of these proteins are very similar, suggesting that it is unlikely that StARD6 would bind more cholesterol on its outer surface than does StARD1.

Proteolytic Digestion and Mass Spectrometric Analysis of StARD6. Whereas the three-dimensional structures of the START domains of StARD3 (*8*) and StARD4 (*9*) are known by X-ray crystallography, and various modeling ventures show a very similar structure for StARD1 (*10*−*12*), nothing is known about the structure of StARD6. Linear amino acid alignments assign StARD6 to a subfamily of START domain proteins containing StARD4, D5, and D6 that is closely related to StARD1 and StARD3 and more distantly related to other START domains (*7*, *16*). As we have previously characterized StARD1 (*37*) and STARD3 (*14*) by partial proteolysis and mass spectrometric analysis of the resulting peptides, we applied the same approach to StARD6 (Figure 3). Digestion with trypsin for 30 min at 4 °C cleaved the full-length protein to a slightly smaller size (Figure 3A, band 1), and to fragments of about 25 kDa (band 2) and about 12 kDa (band 3). These three bands remained stable with digestion up to 60 min at room temperature (Figure 3A). Mass spectrometric analysis of the proteins (Table 3) in these three bands showed that the C-terminus and, to a lesser extent, the N-terminus are protease-sensitive and hence less tightly folded (Figure 3B). In all assays, the first four amino acids (MDYK) were not seen because this peptide was not retained on the trapping column. Analysis of bands 1 and 2 both showed that a carboxyl-terminal domain from residue 196 to the C-terminus had been digested; these bands differed only at their N-termini, having lost either 5 residues (band 1) or 42 residues (band 2). Band 3, which appears to be a single peptide of about 12 kDa in Figure 3A, contained two peptides of 11.7 and 11.9 kDa, comprising residues 29−130 and 123−223, respectively (Figure 3B). By comparing the data from band 3 obtained with 30 min of trypsin at 4 °C to the data obtained after digestion for 60 min at room temperature, it is apparent that the 11.7 kDa peptide from 29 to 130 is more protease-resistant and the 11.9 kDa peptide from 123 to 223 is more protease sensitive. Thus, the overall picture is that the C-terminus of StARD6 is the region that is most sensitive to proteolytic digestion, suggesting it may be more loosely folded and hence accessible to trypsin. This is the same pattern of proteolytic sensitivity previously seen for StARD1 (*37*) and StARD3 (*14*), although StARD6 is distinct in having a smaller protease-sensitive C-terminal region.

To contrast the structures of the C-termini of StARD6 with those of StARD1 and StARD3, we performed a hydropathy

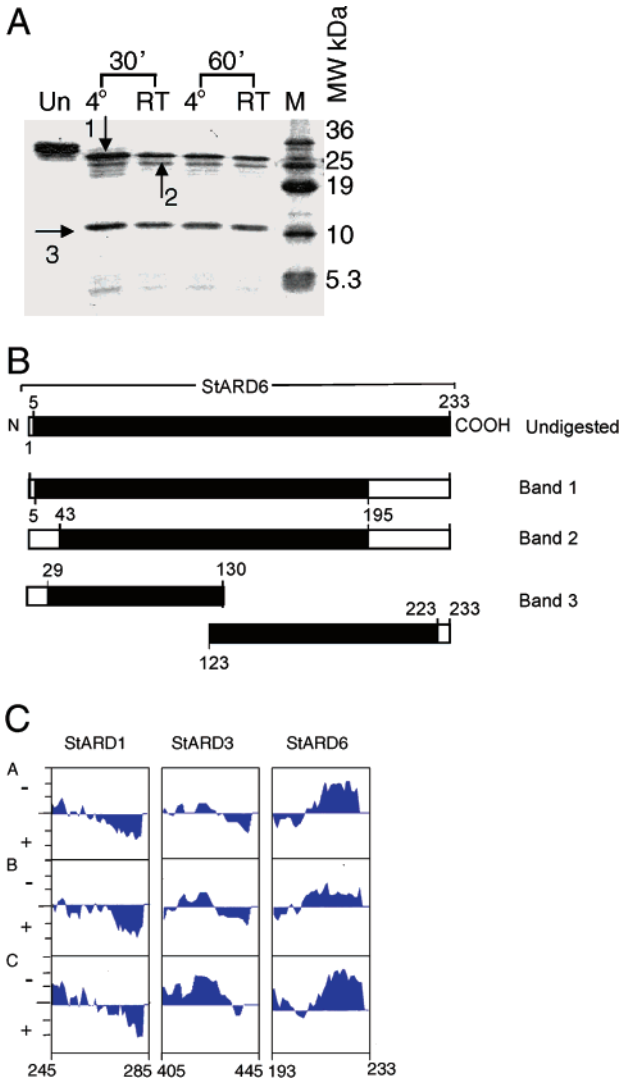

FIGURE 3: Proteolytic digestion of StARD6. Panel A. Tryptic digestion of 5 μg of StARD6 at 4 °C or room temperature (RT) as noted, resolved on 20% SDS−polyacrylamide gel, and stained with Coomassie blue. The protease-resistant bands indicated by the arrows and the undigested band (Un) were excised and analyzed by mass spectrometry. Panel B. Summary of the identified protease-resistant sequences of StARD6. The black region represents the retained amino acids identified by mass spectrometry, and the open region is the protease-sensitive region. The amino acid numbers of relevant cleavage sites are given. Panel C. Hydrophobicity analysis of the StARD1, StARD3, and StARD6 as determined by Fauchere/Pliska hydrophobicity (A), Janin hydrophobicity (B) and Sween/Eisenberg (C) programs. Positive signals (below the line) indicate hydrophilic behavior; negative signals indicate hydrophobic behavior.

analysis of the C-terminal 40 residues of each protein using three different computational programs (Figure 3C). These analyses suggest that the C-termini of StARD1 and StARD3 are hydrophilic, whereas the C-terminus of StARD6 is hydrophobic. The C-terminal 28 residues of StARD1 form an amphipathic helix with acidic residues on the outer surface of the helix that appear to associate with the OMM (*11*). The differences in the hydrophobicity of the C-termini of StARD1 and StARD6 suggest that StARD6 may interact with the OMM by a different mechanism than that used by StARD1, possibly accounting for some of the differences in their activities seen in Figure 2.

Urea Denaturation and Unfolding. To examine potential differences in the stability of StARD1, D3, and D6, we

Table 3: Mass-Spectrometric Analysis of the Trypsin-Resistant Bands

proteins	LC/MS/MS	sequence observed	mass of peptide	proteins	LC/MS/MS	sequence observed	mass of peptide
band 1	5−16	AIAQQTAEQVLA	1241.64	band 2 (contd)	50−60	VEGIIPESAAH	1121.58
	5−17	AIAQQTAEQVLAY	1404.71		50−63	VEGIIPESAAHLSD	1436.71
	18−25	NQDLSGWK	946.44		61−67	LSDLFLK	868.46
	42−49	IFHGNLYR	1018.53		62−67	SDLFLK	755.39
	43−49	FHGNLYR	905.44		80−86	GFNVIHK	813.46
	44−49	HGNLYR	758.37		87−93	IDSDTLI	775.39
	45−49	GNLYR	621.32		87−95	IDSDTLICH	1072.49
	50−56	VEGIIPE	755.40		87−99	IDSDTLICHTITQ	1515.73
	50−58	VEGIIPESA	913.47		96−109	TITQSFAM$_{ox}$GSISPR	1510.75
	50−59	VEGIIPESAA	984.51		110−115	DFIDLV	720.38
	50−60	VEGIIPESAAH	1121.57		110−116	DFIDLVH	857.44
	50−61	VEGIIPESAAHL	1234.64		110−118	DFIDLVHIK	1098.59
	50−63	VEGIIPESAAHLSD	1436.71		112−118	IDLVHIK	836.51
	61−67	LSDFLFK	868.47		113−118	DLVHIK	723.44
	62−67	SDFLFK	755.40		114−118	LVHIK	608.41
	80−86	GFNVIHK	813.45		123−130	NVDIISTK	888.47
	82−86	NVIHK	609.37		124−130	VDIISTK	774.46
	87−93	IDSDTLI	775.40		125−130	DIISTK	675.38
	87−95	IDSDTLICH	1072.49		126−130	IISTK	560.36
	87−99	IDSDTLICHTITQ	1515.72		131−140	SVDFPGYAPT	1052.48
	96−109	TITQSFAM$_{ox}$GSISPR	1510.75		131−143	SVDFPGYAPTSTY	1403.64
	110−115	DFIDLV	720.39		131−145	SVDFPGYAPTSTYIR	1672.81
	110−116	DFIDLVH	857.45		146−154	GFNHPSGYV	976.44
	110−118	DFIDLVHIK	1098.59		146−159	GFNHPSGYVCSPLK	1561.71
	112−118	IDLVHIK	836.53		148−159	NHPSGYVCSPLK	1357.65
	113−118	DLVHIK	723.44		149−159	HPSGYVCSPLK	1243.61
	114−118	LVHIK	608.41		154−159	VCSPLK	702.38
	123−127	NDVII	572.32		155−159	CSPLK	603.31
	123−130	NVDIISTK	888.47		167−176	LVIFVQTEM$_{ox}$K	1222.62
	124−130	VDIISTK	774.46		169−176	IFVQTEM$_{ox}$K	1010.51
	125−130	DIISTK	675.39		170−176	FVQTEM$_{ox}$K	897.44
	126−130	IISTK	560.36		171−176	VQTEM$_{ox}$K	750.37
	131−137	SVDFPGY	783.34		177−186	GKLPASVIEK	1040.62
	131−140	SVDFPGYAPT	1052.47		179−186	LPASVIEK	855.49
	131−143	SVDFPGYAPTSTY	1403.65		180−186	PASVIEK	742.42
	131−145	SVDFPGYAPTSTYIR	1672.80		181−186	ASVIEK	645.38
	134−145	FPGYAPTSTYIR	1371.69		182−186	SVIEK	574.34
	146−153	GFNHPSGY	877.39		187−195	SM$_{ox}$PSNLVSF	996.45
	146−154	GFNHPSGYV	976.44	band 3	5−16	AIAQQTAEQVLA	1241.64
	146−159	GFNHPSGYVCSPLK	1561.72		5−17	AIAQQTAEQVLAY	1404.71
	148−159	NHPSGYVCSPLK	1357.64		18−25	NQDLSGWK	946.44
	149−159	HPSGYVCSPLK	1243.61		42−49	SM$_{ox}$PSNLVSF	1018.53
	154−159	VCSPLK	702.38		42−49	IFHGNLYR	1018.53
	155−159	CSPLK	603.31		45−49	GNYLR	621.33
	167−172	LVIFVQ	717.46		50−60	VEGIIPESAAH	1121.57
	167−176	LVIFVQTEM$_{ox}$K	1222.65		62−67	SDFLFK	755.40
	167−178	LVIFVQTEM$_{ox}$KGK	1407.78		96−109	TITQSFAM$_{ox}$GSISPR	1510.75
	168−176	VIFVQTEM$_{ox}$K	1109.58		110−118	DFIDLVHIK	1098.61
	169−176	IFVQTEM$_{ox}$K	1010.51		113−118	DLVHIK	723.44
	170−176	FVQTEM$_{ox}$K	897.44		123−130	NVDIISTK	888.48
	171−176	VQTEM$_{ox}$K	750.36		124−130	VDIISTK	775.46
	172−176	QTEM$_{ox}$K	651.30		125−130	DIISTK	676.39
	177−186	GKLPASVIEK	1040.61		126−130	IISTK	561.36
	179−186	LPASVIEK	855.49		131−145	SVDFPGYAPTSTYIR	1672.81
	180−186	PASVIEK	742.43		146−159	GFNHPSGYVCSPLK	1561.71
	181−186	ASVIEK	645.38		167−172	LVIFVQ	717.45
	182−186	SVIEK	574.34		167−176	LVIFVQTEM$_{ox}$K	1222.67
	187−195	SM$_{ox}$PSNLVSF	996.46		169−176	IFVQTEM$_{ox}$K	1010.52
band 2	42−49	IFHGNLYR	1018.53		177−186	GKLPASVIEK	1040.62
	43−49	FHGNLYR	905.45		179−186	LPASVIEK	855.50
	44−49	HGNLYR	758.38		180−186	PASVIEK	742.41
	45−49	GNLYR	621.33		181−186	ASVIEK	645.37
	50−56	VEGIIPE	755.41		182−186	SVIEK	574.33
	50−58	VEGIIPESA	913.49		187−195	SM$_{ox}$PSNLVSF	996.46
	50−59	VEGIIPESAA	984.52				

performed urea-mediated unfolding experiments and measured the free energy (ΔG) of stabilization. At higher concentrations of urea, equilibrium unfolding behaviors of StARD1, StARD3, and StARD6 are similar and fit a single exponential (Figure 4A, B, C), and the rates of unfolding are linearly dependent on the denaturant concentration. The apparent fractional extent of protein unfolding was calculated by the equation $f_{app} = ([\theta]_N - [\theta])/([\theta]_N - [\theta]_U)$ (*41*), where $[\theta]_N$ represents the value of the probes in the native state, $[\theta]_U$ represents the values in the unfolded state, and $[\theta]$ is the observed value. Under these conditions, folding appears to be a cooperative transition between the open, unfolded

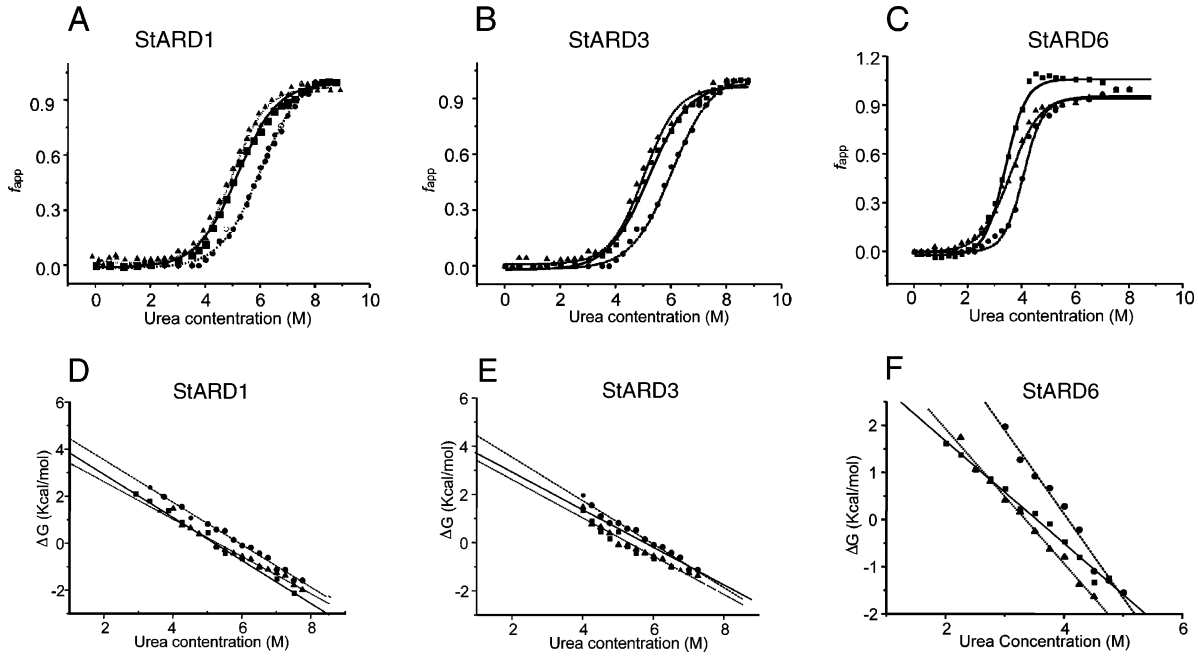

FIGURE 4: Unfolding analysis of the START domains. Panels A−C. The apparent fractional extent of unfolding, f_{app}, was calculated from fluorescence and CD spectra. The squares represent data from the CD spectrum, the triangles represent the fluorescence emission intensity at 320 nm (excitation at 280 nm), and the circles represent the average fluorescence emission wavelength (excitation at 295 nm). Panel A, StARD1; panel B, StARD3; panel C, StARD6. Panels D−F. Measurement of free energy (ΔG) upon urea denaturation. The squares represent the unfolding CD spectrum with the ellipticity value at 228 nm, the circles represent the average fluorescence emission wavelength when excited at 295 nm, and the triangles represent the fluorescence emission intensity at 320 nm when excited at 280 nm. Panel D, StARD1; panel E, StARD3; panel F, StARD6.

state and the tightly packed folded state. By comparing the f_{app} from fluorescence and CD, we can identify three parameters that are similar. The curves for each protein seem to involve two-step unfolding, but the nature of unfolding is different for each protein. For StARD1 and StARD3 (Figure 4A,B), the fluorescence emission intensity, average wavelength, and CD ellipticity remained unchanged up to 3.5 M urea, and the proteins were completely unfolded at 8.0 M urea (a midpoint of 5.75 M). By contrast, the three parameters for StARD6 were stable to 2.0 M urea, and the protein unfolded completely when urea concentrations reached 5.0 M (a midpoint of 3.5 M) (Figure 4C). These results suggest that the active forms of the StARD1, StARD3, and StARD6 proteins have rather minor differences in their unfolding patterns. These results from the fluorescence and CD experiments are similar, and support the hypothesis that a conformational change is necessary for the activity of START proteins.

From the urea-induced unfolding data we calculated the free energy (ΔG) and "*m*", which is proportional to the change in the protein's accessible surface area. We fitted these curves to a two-state model in which the free energy difference between the native (N) and unfolded (U) states depends linearly on the concentration of urea, such that $\Delta G = \Delta G_{H2O} - m[\text{urea}]$ (*41*), where ΔG is the free energy difference at any urea concentration, ΔG_{H2O} is the free energy difference in the absence of urea, and *m* is the solvent denaturant value. ΔG_{H2O} and *m* are determined by a linear extrapolation method (*41*). ΔG determines the stability of a protein, and the *m* value measures the rate of change of ΔG as a function of denaturant concentration. Table 4 and Figure 4D, E, F show the value of ΔG calculated independently from fluorescence intensity, wavelength, and CD. The similarities of the ΔG and *m* values for all three proteins support the hypothesis that the initial and final states of the folding are very similar, and thus the overall energy of stabilization of these proteins is also very similar. These findings are consistent with the view that StARD6 achieves a molten globule conformation similar to StARD1 (*26*, *37*, *42*).

Table 4: Calculation of ΔG and *m* Value

	StARD1*		StARD3		StARD6	
	ΔG	*m*	ΔG	*m*	ΔG	*m*
CD	4.3	1.3	4.8	0.9	3.8	1.1
wavelength	4.3	1.2	5.3	0.9	7.2	1.8
intensity	4.1	0.8	4.2	0.8	4.8	1.4

Real-Time Unfolding of START Domains. To illuminate the mechanism of StARD6 activity, we measured protein unfolding and refolding using stopped-flow spectrophotometry (Figure 5). Stopped-flow devices can monitor the unfolding and refolding of a protein in real time, thus revealing the different kinetic steps involved. The dead time or the mixing time of this instrument is set to 9.3 ms because of the high viscosity of 10 M urea, so that unfolding completed within the 9.3 ms will not be observed. The experiment requires rapid mixing of a protein in buffer with a high concentration of a denaturing agent such as urea or guanidine hydrochloride. High concentrations of urea disrupt the H-bonding of water molecules and thus denature the protein (*43*). Conformational changes in the protein are measured in milliseconds by fluorescence emission following excitation at 295 nm for Trp or at 280 nm for Trp and Tyr. The unfolding kinetics appeared to be a single-exponential process (Figure 5A, C, E), and the values found by extrapolating back to time zero agreed with those for the

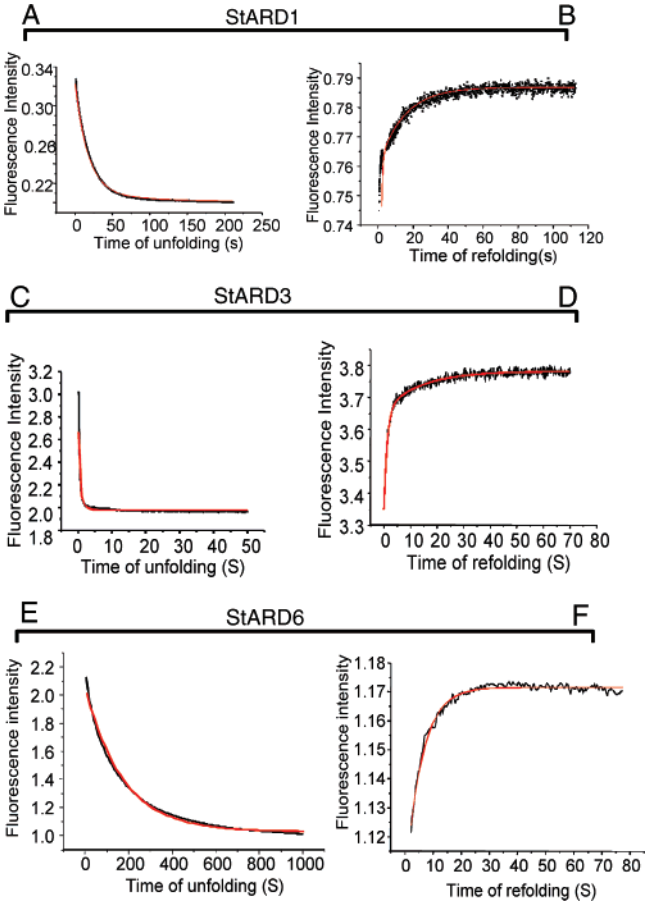

FIGURE 5: Folding and unfolding kinetics determined by stopped-flow fluorescence. The panel indicates the spectrum of each protein: A and B for StARD1, C and D for StARD3, E and F for StARD6. The panels A, C, and E are the unfolding experiments and B, D, and F are refolding experiments.

native-state of the protein. When the denaturant is suddenly mixed, the protein starts to unfold. The rapid unfolding phase is defined as the "burst phase", which may or may not entail complete unfolding. When the unfolding is completed, there is no change in fluorescence emission. The unfolding of StARD1 occurred after the burst phase, not within the dead time. As measured by fluorescence emission, the time of unfolding was 16.9 s with a relaxation time of 77 s (Figure 5A), demonstrating that StARD1 unfolds by a two-step process. Under similar conditions, the unfolding of StARD6 is slower, with an initial relaxation of 48 s and a final relaxation of 232 s (Figure 5E). Thus, the initial transient state of StARD6 unfolding is quite slow, and the relaxation time required for the complete unfolding is long, so that the unfolding of StARD6 is slower than the unfolding of StARD1. This slow unfolding suggests that there are no rearrangements during unfolding (*44*). Like the unfolding kinetics, the refolding kinetics of StARD6 was slower than that of StARD1 (Figure 5B,F). StARD3 was refolded in 14 s (Figure 5D), a time that is similar to the unfolding kinetics of StARD1.

StARD6 Associates More Stably with the OMM Than StARD1. The activity data and unfolding experiments showed that slower unfolding increased activity. Because the unfolding of StARD1 and StARD6 at the mitochondrial membrane is slow, it is difficult to imagine how these proteins can be induced to unfold at the mitochondrial membrane to mediate

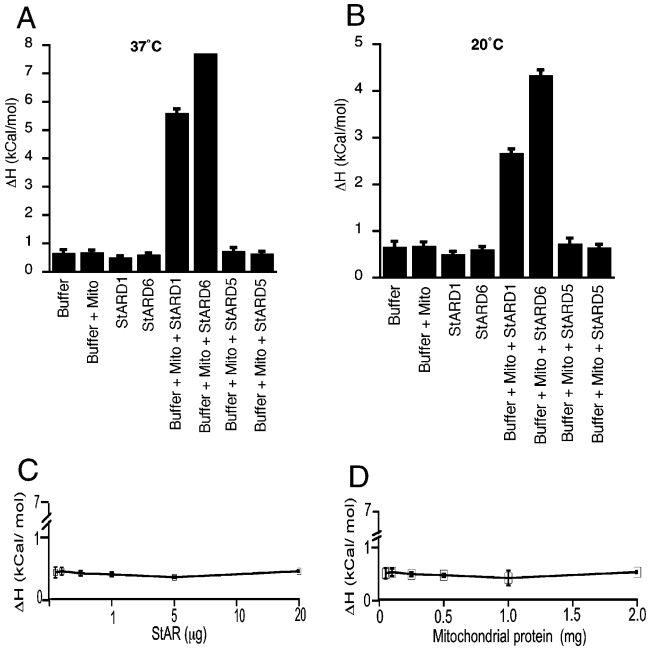

FIGURE 6: Isothermal titration calorimetry. The change in enthalpy (ΔH) was measured following the addition of StARD1, StARD3, or StARD6 to 300 μg of mitochondrial protein. Panel A, data at 37 °C; panel B, data at 20 °C. The control experiments were performed under identical conditions with cholesterol and StAR (panel C) or mitochondria and cholesterol (panel D).

cholesterol transport into the mitochondria. StARD4, D5 and D6 do not have identifiable signal sequences, and StARD1 and StARD3 are active without entering into the mitochondria (*14*, *24*, *37*). Therefore, we predict that the active conformation of the START domain is attained in association with the OMM. However, empirical evidence supporting this prediction is lacking. To test this hypothesis, we measured the enthalpy (ΔH) of interaction between START proteins and mitochondrial membranes by titration calorimetry. We found that the interaction between StARD6 and the mitochondria was more stable than the interaction between StARD1 and the mitochondria. Reducing the temperature from 37 °C to 4 °C did not stop the conversion of cholesterol to pregnenolone (*45*), but it did decrease the ΔH. At 37 °C, the ΔH values for StARD1 and StARD6 were 5.6 and 7.7 kcal/mol, respectively (Figure 6A). Reducing the temperature from 37 °C to 20 °C reduced ΔH by 53% (2.66 ± 0.13 kcal/mol) for StARD1 and 44% for StARD6 (4.33 kcal/mol) (Figure 6B). Decreasing the temperature further to 10 °C reduced the ΔH of both StARD1 and StARD6 to 2.26 ± 0.11 kcal/mol (not shown). Increasing amounts of StAR (Figure 6C) or mitochondrial protein (Figure 6D) did not affect the ΔH, which is similar to the ΔH of the buffer control (Figure 6A and 6B). Therefore, the change in heat content for StARD6 in association with the OMM is more than that of StARD1.

Computational Modeling of StARD6. The structure of mouse StARD6 was modeled based on the crystal structure of mouse StARD4 and validated with Procheck (*46*, *47*) and What If (*48*) programs (Figure 7). The root-mean-square for bond length relative to common refinement constraint values was 0.704 Å, and for the bond angles was 1.260°. The Ramachandran plots of all residues show that 205 residues (88.7%) were in the favored region, 21 residues (9.1%) were in the allowed region and 5 residues (2.2%) were in the

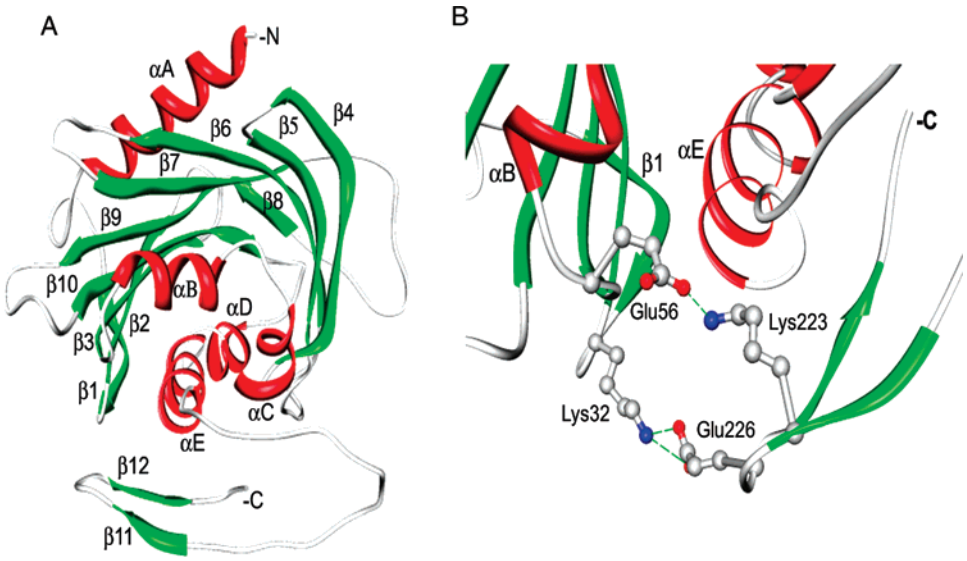

FIGURE 7: Ribbon diagram of the structural model of StARD6. Panel A. Overview of the whole protein. The N-terminal helix is in the upper right-hand corner; the C-terminal helices are in the lower center, the C-tail is extended out of the plane of the diagram. β-sheets are labeled 1−12 and α-helices A−E. Panel B. Image of the interaction of the C-tail with the main structure of StARD6. During the 100 ps MD simulation, the C-tail formed two salt bridges with the main structure. The salt bridges between Lys223 and Glu56 and between Glu226 and Lys32 are shown as ball-and-stick representations (white, carbon; blue, nitrogen; red, oxygen). Hydrogen bonds are shown in dashed green lines.

general allowed region. The free energy of the model was -5.08×10^3 kcal/mol after energy minimization with the Amber7 program (*33*), which was similar to the value of -6.29×10^3 kcal/mol calculated under the same condition for the crystal structure of StARD4.

Except for the C-tail (residues 210−233), the predicted overall structure of StARD6 was remarkably similar to the crystal structures of both StARD3 and StARD4. The barrel of the putative sterol-binding pocket was formed by 10 twisted antiparallel β-sheets (with the exception of β9, which was a continuation of β8), stretched by the long N-terminal α-helix (termed αA) and parallel C-terminal α-helices (termed αD and αE) at each end (Figure 7A). Two short α-helices, αB and αC, each with two turns, lie above the C-helices and form the front of the sterol-binding pocket (SBP). StARD4 also has the conserved salt bridge pair (Lys67−Asp113) inside the SBP, which may play a role in lipid binding as well as stabilizing the structure.

The most significant difference between StARD6 and StARD4 was at the C-terminal region. The C-terminal region encompassing the C-helix in StARD4 was broken into two shorter α-helices: αD and αE in StARD6. The C-tail region of StARD6 forms a *z*-shape extension from αE with two short antiparallel β-truns at the end. In the static model, the C-helical region of StARD6 was composed of two shorter helices: residues 181−187 and 192−202. The Asp106−Arg272 salt bridge pair in StARD1, which may play a role in regulating the movement of C-helix (*26*), is not found in StARD6. Pairs of such residues were also conserved in the crystal structures of StARD3 (Asp269−Arg435) (*8*) and StARD4 (Asp53−Arg218) (*9*). Furthermore, the C-helices of StARD6 did not form salt bridges with the main structure, but rather interacted with the main structure through hydrogen bond networks among residues Glu185−Tyr48, Asn191−Ser77 and Lys200−Ile53. These loose interactions and the break in the C-helices may increase the flexibility of the C-helices, allowing structural rearrangement of the putative SBP.

In the static model, the C-tail forms an extension following αE and interacts with the main structure through hydrogen bond networks involving residues Lys223−Val203, Glu226−Tyr164 and Ile231−Asp201. During the MD run, the C-tail interacted with the main structure and formed salt bridges at Lys223−Glu56 (the turn between β3-sheet and αB) and Glu226−Lys32 (the short turn between β1- and β2-sheets) (Figure 7B), indicating that the C-tail might play a role in stabilizing the main structure. The C-tail was hydrophilic, containing 10 positively charged residues, including 3 His residues. It is not clear how this C-tail might affect StARD6 activity. Its loose structure probably exerts little restriction on the movements of the C-helices, but maintains overall protein folding through the charged interactions.

DISCUSSION

Our data show that StARD6 exhibits full StAR-like activity to induce steroidogenesis in isolated mitochondria in vitro. It can bind cholesterol better than StARD1 and is folded similarly to StARD1. Our biophysical experiments show that StARD1 and StARD6 have very similar patterns of unfolding and refolding, but that StARD6 undergoes these changes more slowly. Calorimetry data showed that StARD6 interacts with mitochondria in a more stable fashion than does StARD1; we propose that this more stable interaction correlates with the greater ability of StARD6 to promote mitochondrial cholesterol import.

The unfolding and refolding of both StARD1 and StARD6 are slow and require interaction with the OMM, where StAR exerts its activity. The nature of the unfolding of StAR-like proteins to induce steroidogenesis remains somewhat controversial. Based on changes in the CD spectrum, fluorescence spectroscopy and pattern of partial proteolysis of StARD1 as a function of pH, we proposed that StARD1 acts

on the OMM as a molten globule (*37*). We subsequently confirmed that StARD1 acts exclusively on the OMM (*24*), and others have characterized the selective intramitochondrial degradation of StARD1 by *lon* protease (*49*, *50*). Subsequent work using molecular dynamic imaging of StARD1 showed that the overall structure of StARD1 remained stable under acidic conditions, but that several segments of the protein underwent conformational changes (*26*). The most dramatic pH-induced change is the movement of the C-terminal helix, which opens and closes the access to the sterol-binding pocket. Preventing the movement of the C-helix by creating a disulfide bond linking it to an adjacent structure eliminated the CD signature of the molten globule and eliminated cholesterol binding and StAR-like activity. Activity could be restored by cleaving the disulfide bond, showing that it is the immobilization of the C-helix, and not the amino acid replacement, that eliminated activity (*26*). Thus the present view of the molten globule model of StAR action is that the structural change required for protein activity is movement of the C-helix, and not unfolding of the whole protein (*26*, *40*). Our present data with StARD6 show biophysical behavior and structure that is very similar to that of StARD1 and indicate that StARD6 undergoes a similar molten globule conformational change when it exerts activity on the OMM. Both StARD1 and StARD6 have similar changes in free energy when undergoing transient partial unfolding (Figure 4), both unfold with similar kinetics (Figure 5), both show a dramatic increase in enthalpy when associating with the OMM (Figure 6), and both have similar predicted structures (Figure 7). Thus we propose that both StARD1 and StARD6 act as molten globules on the OMM to induce the movement of cholesterol from the OMM to the IMM.

While much has been established about the requirements for StAR-like activity on the OMM, the precise mechanism of this activity remains unknown (*51*). It is most likely that StAR's action on the OMM requires interaction with OMM proteins, possibly by associating with the peripheral benzodiazepine receptor complex (*52*). Confusion has arisen because StAR can bind cholesterol and transfer it between membrane systems in vitro, suggesting that StAR acts by transferring cholesterol from cytoplasmic sources to the OMM (*53*, *54*). However, this in vitro cholesterol binding and transfer activity is retained by a StAR mutant (R182L) that is devoid of StAR activity and causes congenital lipoid adrenal hyperplasia (*40*). Thus considerations of StAR activity must carefully distinguish between its activity to transfer cholesterol between membranes and its activity to induce steroidogenesis by increasing the movement of cholesterol from the OMM to the IMM. This distinction is also seen with StARD6, as cholesterol binding activity was clearly greater than that of StARD1 or StARD3 (Figure 2E), but activity was equivalent (Figure 2A).

Sequence similarity studies show that StARD6 belongs to a subfamily of StARD proteins that includes StARD4 and StARD5 (*14*, *20*), which, respectively, have little or no StAR-like activity (*21*). It has been proposed that StARD4 and StARD5 act to facilitate the trans-cytoplasmic movement of cholesterol (which is otherwise nearly insoluble) from intracellular cholesterol stores in lipid droplets to various membranes (cholesterol-transfer activity) (*7*) and StARD5 can bind cholesterol in vitro (*55*). Such a function would be consistent with their lack of recognizable leader peptides that would target these proteins to specific organelles. StARD6 similarly can bind cholesterol and lacks a recognizable leader peptide, hence we propose that StARD6 is a bifunctional protein, possessing both cholesterol-transfer activity and, as shown above, StAR-like activity. However, as StARD6 expression is confined to the male germ cell line, it cannot substitute for the function of StARD1.

ACKNOWLEDGMENT

We thank Dr. Michael Field from the School of Animal Sciences for the pig adrenal tissues, Dr. Charles Wood from the Department of Physiology for the generous support of the adrenal tissues from his experimental animals, Dr. Jan Breslow for the mouse StARD4, StARD5, and StARD6 plasmids, and Dr. S Granti for the StARD7 plasmid. The authors are also thankful to Drs. Arther Edison and Joanna Long for the calorimetry, CD, and stopped-flow instruments.

REFERENCES

1. Stocco, D. M., and Clark, B. J. (1996) Regulation of the acute production of steroids in steroidogenic cells, *Endocr. Rev. 17*, 221−244.
2. Lin, D., Sugawara, T., Strauss, J. F., III, Clark, B. J., Stocco, D. M., Saenger, P., Rogol, A., and Miller, W. L. (1995) Role of steroidogenic acute regulatory protein in adrenal and gonadal steroidogenesis, *Science 267*, 1828−1831.
3. Bose, H. S., Sugawara, T., Strauss, J. F., III, and Miller, W. L. (1996) The pathophysiology and genetics of congenital lipoid adrenal hyperplasia, *N. Engl. J. Med. 335*, 1870−1878.
4. Caron, K. M., Soo, S.-C., Wetsel, W. C., Stocco, D. M., Clark, B. J., and Parker, K. L. (1997) Targeted disruption of the mouse gene encoding steroidogenic acute regulatory protein provides insights into congenital lipoid adrenal hyperplasia, *Proc. Natl. Acad. Sci. U.S.A. 94*, 11540−11545.
5. Hasegawa, T., Zhao, L., Caron, K. M., Majdic, G., Suzuki, T., Shizawa, S., Sasano, H., and Parker, K. L. (2000) Developmental roles of the steroidogenic acute regulatory protein (StAR) as revealed by StAR knockout mice, *Mol. Endocrinol. 14*, 1462−1471.
6. Ponting, C. P., and Aravind, L. (1999) START: a lipid-binding domain in StAR, HD-ZIP and signalling proteins, *Trends Biochem. Sci. 24*, 130−132.
7. Soccio, R. E., and Breslow, J. L. (2003) StAR-related lipid transfer (START) proteins: mediators of intracellular lipid metabolism, *J. Biol. Chem. 278*, 22183−22186.
8. Tsujishita, Y., and Hurley, J. H. (2000) Structure and lipid transport mechanism of a StAR-related domain, *Nat. Struct. Biol. 7*, 408−414.
9. Romanowski, M. J., Soccio, R. E., Breslow, J. L., and Burley, S. K. (2002) Crystal structure of the Mus musculus cholesterol-regulated START protein 4 (StarD4) containing a StAR-related lipid transfer domain, *Proc. Natl. Acad. Sci. U.S.A. 99*, 6949−6954.
10. Mathieu, A., Fluery, A., Ducharme, L., Lavige, P., and LeHoux, J. (2002) Insights into steroidogenic acute regulatory protein (StAR)-dependent cholesterol transfer in mitochondria: evidence from molecular modeling and structure-based thermodynamic supporting the existence of partially unfolded states of StAR, *J. Mol. Endocrinol. 29*, 327−345.
11. Yaworsky, D. C., Baker, B. Y., Bose, H. S., Best, K. B., Jensen, L. B., Bell, J. D., Baldwin, M. A., and Miller, W. L. (2005) pH-dependent Interactions of the carboxyl-terminal helix of steroidogenic acute regulatory protein with synthetic membranes, *J. Biol. Chem. 280*, 2045−2054.
12. Murcia, M., Faraldo-Gomez, J. D., Maxfield, F. R., and Roux, B. (2006) Modelling the structure of the StART domains of MLN64 and StAR proteins in complex with cholesterol, *J. Lipid Res. 47*, 2614−2630.
13. Watari, H., Arakane, F., Moog-Lutz, C., Callen, C. B., Tomasetto, C., Gerton, G. L., Rio, M. C., Baker, M. E., and Strauss, J. F., III (1997) MLN64 contains a domain with homology to the steroidogenic acute regulatory protein (StAR) that stimulates steroidogenesis, *Proc. Natl. Acad. Sci. U.S.A. 94*, 8462−8467.

14. Bose, H. S., Whittal, R. M., Huang, M. C., Baldwin, M. A., and Miller, W. L. (2000) N-218 MLN64, a protein with StAR-like steroidogenic activity is folded and cleaved similarly to StAR, *Biochemistry 39*, 11722−11731.
15. Soccio, R. E., Adams, R. M., Maxwell, K. N., and Breslow, J. L. (2005) Differential gene regulation of StarD4 and StarD5 cholesterol transfer proteins. Activation of StarD4 by sterol regulatory element-binding protein-2 and StarD5 by endoplasmic reticulum stress, *J. Biol. Chem. 280*, 19410−19418.
16. Alpy, F., and Tomasetto, C. (2005) Give lipids a START: the StAR-related lipid transfer (START) domain in mammals, *J. Cell Sci. 118*, 2791−2801.
17. Gomes, C., Oh, S. D., Kim, J. W., Chun, S. Y., Lee, K., Kwon, H. B., and J., S. (2005) Expression of the putative sterol binding protein StARD6 gene in male cell specific, *Biol. Reprod. 72*, 651−658.
18. Soccio, R. E., Adams, R. M., Romanowski, M. J., Sehayek, E., Burley, S. K., and Breslow, J. L. (2002) The cholesterol-regulated StarD4 gene encodes a StAR-related lipid transfer protein with two closely related homologues, StarD5 and StarD6, *Proc. Natl. Acad. Sci. U.S.A. 99*, 6943−6948.
19. Gill, S. C., and von Hippel, P. H. (1989) Calculation of protein extinction coefficients from amino acid sequence data, *Anal. Biochem. 182*, 319−326.
20. Sreerama, N., Venyaminov, S. Y., and Woody, R. W. (2000) Estimation of secondary structure from circular dichroism spectra: inclusion of denatured proteins with native proteins in the analysis, *Anal. Biochem. 287*, 243−251.
21. Sreerama, N., and Woody, R. W. (1993) A self-consistent method for the analysis of protein secondary structure from circular dichroism, *Anal. Biochem. 209*, 32−44.
22. Sreerama, N., and Woody, R. W. (2000) Estimation of protein secondary structure from CD spectra: Comparison of CONTIN,-SELCON and CDSSTR methods with an expanded reference set, *Anal. Biochem. 282*, 252−260.
23. Sreerama, N., and Woody, R. W. (2004) Computation and alalysis of protein circular dichroism spectra, *Methods Enzymol. 383*, Chapter 13, 383−318.
24. Bose, H. S., Lingappa, V. R., and Miller, W. L. (2002) Rapid regulation of steroidogenesis by mitochondrial protein import, *Nature 417*, 87−91.
25. Petrescu, A. D., Gallegos, A. M., Okamura, Y., Strauss, J. F., III, and Schroeder, F. (2001) Steroidogenic acute regulatory protein binds cholesterol and modulates mitochondrial membrane sterol domain dynamics, *J. Biol. Chem. 276*, 36970−36982.
26. Baker, B. Y., Yaworsky, D. C., and Miller, W. L. (2005) A pH-dependent molten-globule transition is required for activity of the steroidogenic acute regulatory protein, StAR, *J. Biol. Chem. 280*, 41753−41760.
27. Rosenfeld, J., Capdeville, J., Guillemot, J. C., and Ferrara, P. (1992) In-gel digestion of proteins for internal sequence analysis after one- or two-dimensional electrophoresis, *Anal. Biochem. 203*, 173−179.
28. Eftink, M. R., and Ghiron, C. A. (1981) Fluorescence quenching studies with proteins, *Anal. Biochem. 114*, 199−227.
29. Eftink, M. R. (1991) Fluorescence techniques for studying protein structure, *Methods Biochem. Anal. 35*, 127−205.
30. Enoki, S., Maki, K., Inobe, T., Takahashi, K., Kiyoto, K., Oroguchi, T., Nakatani, H., Tomoyori, K., and Kuwajima, K. (2006) The equilibrium unfolding observed at pH 4 and its relationship with the kinetic folding in green fluorescent protein, *J. Mol. Biol. 361*, 969−982.
31. Darley-Usmer, V. M., Rickwood, D., and Wilson, M. T. (1986) *Mitochondria a practical approach*, IRL Press, Cary, NC.
32. Sali, A., and Blundel, T. L. (1993) Comparative protein modeling by satisfaction of spatial restraints, *J. Mol. Biol. 234*, 779−815.
33. Case, D. A., Pearlman, D. A., Caldwell, T. E., Cheatham, I., Wang, J. L., Ross, W. S., Simmerling, C. L., Darden, T. A., Merz, K. M., Staton, R. V., Cheng, A. L., Vincent, J. J., Crowley, V., Tsui, H., Gohlke, R. J., Duan, Y., Pitera, J., Massova, I., Seibel, G. L., Singh, U. C., Weiner, P. K., and Kollman, P. A. (1992) *Amber 7*, University of California, San Francisco.
34. Cornell, W. D., Cieplak, P., Bayly, C. I., Gould, R. I., Merz, K. M., Ferguson, D. M., Spellmeyer, D. C., Fox, T., Caldwell, J. W., and Kollman, P. A. (1995) A second generation force field for the simulation of proteins, nucleic acids, and organic molecules, *J. Am. Chem. Soc. 117*, 5179−5197.
35. Petterson, E., Goddard, T., Huang, C., Couch, G., Greenblatt, D., Meng, E., and Ferrin, T. (2004) UCSF-Chimera−A visualization system for exploratory research and analysis, *J. Comput. Chem. 25*, 1605−1612.
36. Bose, H. S., Baldwin, M. A., and Miller, W. L. (1998) Incorrect folding of steroidogenic acute regulatory protein (StAR) in congenital lipoid adrenal hyperplasia, *Biochemistry 37*, 9768−9775.
37. Bose, H. S., Whittal, R. M., Baldwin, M. A., and Miller, W. L. (1999) The active form of the steroidogenic acute regulatory protein, StAR, appears to be a molten globule, *Proc. Natl. Acad. Sci. U.S.A. 96*, 7250−7255.
38. Fasman, G. D., (Ed.) (1996) *Circular dichroism and the conformational analysis of biomolecules*, Plenum Press, New York.
39. King, S. R., Smith, A. G., Alpy, F., Tomasetto, C., Ginsberg, S. D., and Lamb, D. J. (2006) Characterization of the putative cholesterol transport protein metastatic lymph node 64 in the brain, *Neuroscience 139*, 1031−1038.
40. Baker, B. Y., Epand, R. F., Epand, R. M., and Miller, W. L. (2007) Cholesterol binding does not predict activity of the steroidogenic acute regulatory protein, *J. Biol. Chem. 282*, 10223−10232.
41. Pace, C. N. (1986) Determination and analysis of urea and guanidine hydrochloride denaturation curves, *Methods Enzymol. 131*, 266−280.
42. Privalov, P. L. (1996) Intermediate states in protein folding, *J. Mol. Biol. 258*, 707−725.
43. Baldwin, R. L. (1993) Finding intermediates in protein folding, *Bioessays 16*, 207−210.
44. Agashe, V. R., Shastry, M. C., and Udgaonkar, J. B. (1995) Initial hydrophobic collapse in the folding of barstar, *Nature 377*, 754−757.
45. Paul, D. P., Gallant, S., Orme-Johnson, N. R., Orme-Johnson, W. H., and Brownie, A. C. (1976) Temperature dependence of cholesterol binding to cytochrome P-450scc of the rat adrenal, *J. Biol. Chem. 251*, 7120−7126.
46. Laskowski, R. A., MacArthur, M. W., Moss, D. S., and Thornton, J. M. (1993) PROCHECK−a program to check the stereochemical quality of protein structures, *J. Appl. Crystallogr. 26*, 283−291.
47. Morris, A. L., MacArthur, M. W., Hutchinson, E. G., and Thorton, J. S. (1992) Stereochemical quality of protein structure coordinates, *Proteins 12*, 345−364.
48. Vriend, G. (1990) WHAT IF: A molecular modeling and drug design program, *J. Mol. Graphics 8*, 52−56.
49. Granot, Z., Geiss-Friedlander, R., Melamed-Brook, N., Eimerl, S., Timberg, R., Weiss, A. M., Hales, K. H., Hales, D. B., Stocco, D. M., and Orly, J. (2003) Proteolysis of normal and mutated steroidogenic acute regulatory proteins in the mitochondria; the fate of unwanted proteins, *Mol. Endocrinol. 17*, 2461−2476.
50. Granot, Z., Kobiler, O., Melamed-Book, N., Eimerl, S., Bahat, A., Lu, B., Braun, S., Maurizi, M. R., Suzuki, C. K., Oppenheim, A. B., and Orly, J. (2007) Turnover of mitochondrial steroidogenic acute regulatory (StAR) protein by Lon protease: the unexpected effect of proteasome inhibitors, *Mol. Endocrinol. 21*, 2164−2177.
51. Miller, W. L. (2007) StAR search−what we know about how the steroidogenic acute regulatory protein mediates mitochondrial cholesterol import, *Mol. Endocrinol. 21*, 589−601.
52. Hauet, T., Yao, Z.-X., Bose, H. S., Wall, C. T., Han, Z., Li, W., Hales, D. B., Miller, W. L., Culty, M., and Papadopoulos, V. (2005) Peripheral-Type benzodiazepine receptor-mediated action of steroidogenic acute regulatory protein on cholesterol entry into leydig cell mitochondria, *Mol. Endocrinol. 19*, 540−554.
53. Kallen, C. B., Billheimer, J. T., Summers, S. A., Stayrook, S. E., Lewis, M., and Strauss, J. F., III (1998) Steroidogenic acute regulatory protein (StAR) is a sterol transfer protein, *J. Biol. Chem. 273*, 26285−26288.
54. Tuckey, R. C., Headlam, M. J., Bose, H. S., and Miller, W. L. (2002) Transfer of Cholesterol between Phospholipid Vesicles Mediated by the steroidogenic acute regulatory protein (StAR), *J. Biol. Chem. 277*, 47123−47128.
55. Rodriguez-Agudo, D., Ren, S., Hylemon, P. B., Redford, K., Natarajan, R., Del Castillo, A., Gil, G., and Pandak, W. (2005) Human StARD5, a cytosolic StAR-related binding protein, *J. Lipid Res. 46*, 1615−1623.

BI701966A